Dyes and Pigments 83 (2009) 339–347

Contents lists available at ScienceDirect

Dyes and Pigments

journal homepage: www.elsevier.com/locate/dyepig

The synthesis, physicochemical properties and anodic polymerization of a novel ladder pentaphenylene

Nicolas Cocherel [a,b], Cyril Poriel [a,b,*], Olivier Jeannin [a,b], Ali Yassin [a,b], Joëlle Rault-Berthelot [a,b,**]

[a] Université de Rennes 1, Bat 10C, Campus de Beaulieu, 35042 Rennes cedex France
[b] UMR CNRS 6226, "Sciences Chimiques de Rennes" – MaCSE group, France

ARTICLE INFO

Article history:
Received 16 March 2009
Received in revised form
28 May 2009
Accepted 1 June 2009
Available online 16 June 2009

Keywords:
Ladder phenylene materials
Spiroconjugation
Optical properties
Blue light emission
Structure–properties relationship
Electropolymerization

ABSTRACT

The synthesis, crystal structure, electrochemical and optical properties of a novel blue emitting ladder pentaphenylene are reported and compared with those of its 3π–2 spiro parent, in order to study the effect of the spiro-linked fluorene rings. Anodic oxidation of the novel compound results via electropolymerization, in the formation of an electroactive material that displays interesting electrochemical and optical properties.

1. Introduction

Organic semiconductors (small molecules or polymers) have been extensively studied as materials for organic light-emitting diodes (OLED), photovoltaic cells and field-effect transistors (OFET) [1]. Phenylene-based π-conjugated systems are one of the most important class of conjugated materials for organic electronic applications due to their efficient blue emission, which make them highly attractive for use in OLED [2]. For the last ten years, the Müllen group have designed numerous materials for organic electronics and especially ladder type phenylenes have been widely used as efficient blue emitters for OLED [3–7] or for solar cells applications [8].

Despite the recent progress in term of stability for blue OLEDs [9–19], it is still highly challenging to prepare efficient materials, possessing a wide band gap fitting for a blue emission and that might be used in a single layer device to avoid complicated multilayer architecture [18]. The control of properties by synthetic design, for polymers as well as for oligomers, is thus highly important. For example, in oligo/poly(ladder-phenylene) the properties can be tuned by the nature of the bridges e.g. C, N, S, Si etc… [2]. In this context, a structure/property relationship approach is nowadays essential in order to design such highly efficient materials. For the last two years, our group has designed new classes of UV and blue emitters called DiSpiroFluorene–IndenoFluorene (**DSF–IF**) (Fig. 1) [20–22]. These fluorophores present a general 3π–2 spiro architecture, in which the central π-system 1 i.e. indenofluorene (**IF**) [23] is spiro-linked to two fluorene units *i.e.* π-systems 2. In order to go deeper in the knowledge of the properties of the **DSF–IF** core, we recently investigated the physicochemical properties of the central unit **IF**, *i.e* the π-system 1 in **DSF–IF** (Fig. 1, left) [20]. That leads us to improve the understanding of the electrochemical/optical properties of **DSF–IF**s and the influence of the two spiro-linked fluorene units on the central core [20]. Using the same molecular design, we recently prepared a new fluorophore for blue OLED applications called DiSpiroFluorene Ladder PentaPhenylene (**DSF–LPP**), in which the conjugation of the fused central π-system 1 was increased i.e. 5 phenyl rings instead of 3 (in order to tune the emission colour) and in which alkyl chains were incorporated to increase the solubility (Fig. 1, right) [24]. The two spiro-linked fluorenes were kept unchanged. As a development to our previous investigations in the **IF** series, and to go deeper in the knowledge of aromatic fused compounds and spiroconjugation, we

* Corresponding author. Tel.: +33 0 223235977; fax: +33 0 223236732.
** Corresponding author. Tel.: +33 0 223235964; fax: +33 0 223236732.
E-mail addresses: cyril.poriel@univ-rennes1.fr (C. Poriel), joelle.rault-berthelot@univ-rennes1.fr (J. Rault-Berthelot).

0143-7208/$ – see front matter
doi:10.1016/j.dyepig.2009.06.001

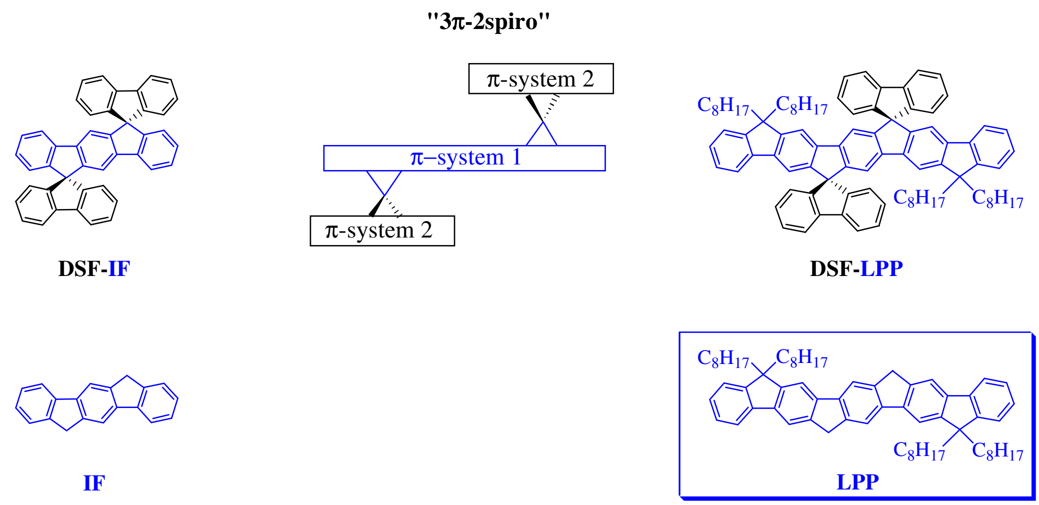

Fig. 1. 3π−2spiro concept in **DSF–IF** and **DSF–LPP** and their corresponding π-system building block i.e. **IF** and **LPP**.

investigate now a new ladder pentaphenylene (**LPP**), which is one of the simplest bridged ladder type pentaphenylene ever prepared, bearing only, in the two extremities, two octyl chains for solubility purposes. **LPP** is thus an attractive model compound as it can be seen as the central π-system 1 of the **DSF–LPP** and other pentaphenylenes [3,6,25,26]. This study may offer a useful way to improve the understanding of the physico-chemical properties in a variety of conjugated macromolecules for optoelectronics applications. For example, a usual thinking on polyfluorenes is that the substitutions at the bridges are only important to control the interactions between the polymer chains and the environment but do not influence the electronic properties. However, it is known, in spiro molecules, that the two orthogonally π systems may interact, which modify the previous approach [27,28]. Herein, we thus reported the synthesis, X-ray structure, optical and electrochemical properties of **LPP**, together with the comparison with its di-spiro parent, **DSF–LPP** (to study the spiro-linked fluorene effects through the spiroconjugation), and with the indenofluorene series (**DSF–IF** and **IF**). Moreover, as observed for numerous fluorene (**F**) derivatives [29], and **IF** derivative [30] anodic oxidation of **LPP** leads, through electropolymerization process, to the formation of an electroactive material, with interesting electrochemical and optical properties.

2. Experimental

2.1. Synthesis

Light petroleum refers to the fraction with bp 40–60 °C. Reactions were stirred magnetically, unless otherwise indicated. Analytical thin layer chromatography was carried out using aluminium backed plates coated with Merck Kieselgel 60 GF_{254} and visualized under UV light (at 254 and/or 365 nm). Chromatography was carried out using silica 60A CC 40–63 μm (SDS). ^1H and ^{13}C NMR spectra were recorded using Bruker 300 MHz instruments (^1H frequency, corresponding ^{13}C frequency is 75 MHz); chemical shifts were recorded in ppm and *J* values in Hz. In the ^{13}C NMR spectra, signals corresponding to CH, CH_2 or Me groups, assigned from DEPT, are noted; all others are C. The residual signals for the NMR solvents are: $CDCl_3$: 77.00 ppm for the carbon; CD_2Cl_2: 5.32 ppm for the proton; The following abbreviations have been used for the NMR assignment: s for singlet, d for doublet, t for triplet and m for multiplet. High resolution mass spectra were recorded either at the Centre Régional de Mesure Physique de l'Ouest (Rennes) or with a Microflex LT (Bruker). Di-ester **1** was prepared according to a modified Tour procedure starting from 1,4-dibromo-2,5-dimethylbenzene in a two-step oxidation reaction followed by an esterification [24,31]. 9,9-dioctylfluorene-2-boronate ester **2** has been prepared according to literature procedures starting from commercially available 2-bromofluorene [32–34]. The diketone **3** was prepared as we previously reported [24].

2.1.1. LPP

Potassium hydroxide (150 mg, 2.67 mmol) was added to a stirred solution of the diketone **3** (100 mg, 0.11 mmol) in suspension in diethylene glycol (12 ml) at room temperature. Hydrazine monohydrate [editors note: toxic; incompatible with a wide variety of materials, including oxidizing agents, heavy metal oxides, dehydrating agents, alkali metals, rust, silver salts; combustible; contact with many materials may result in explosive decomposition; vapour highly may combust explosively] (98%, 160 μL, 3.22 mmol) was added via a syringe and the schlenk tube was degassed. The reaction mixture was vigorously stirred at 180 °C, under an argon atmosphere for 20 h. The hot solution was then poured into ice containing hydrochloric acid. The mixture was extracted with dichloromethane (3 × 20 mL) and the extracts were dried ($MgSO_4$). The solvent was removed in vacuo and the residue was purified by column chromatography on silica gel eluting with dichloromethane/light petroleum (1:9) to give the title compound **LPP** (63 mg, 65%) as a slightly yellow solid. mp 138 °C, (Found C, 90.07; H, 9.91. $C_{66}H_{86}$ requires C, 90.14; H, 9.86%) (Found $[M]^{+\cdot}$, 878.6724. $C_{66}H_{86}$ requires 878.67295); ν_{max} (KBr)/cm^{-1} = 3050, 3006, 2925, 2852, 1607, 1463, 1421, 1180, 849; λ_{max} CH_2Cl_2/nm 386 (ε 360797), 366 (238 122), 329 (51 741); δ_H (300 MHz; CD_2Cl_2) 8.02 (2H, s, ArH), 7.90 (2H, s, ArH), 7.80 (2H, s, ArH), 7.74 (2H, d, *J* 7.5, ArH), 7.39–7.27 (6H, m, ArH), 4.06 (4H, s, CH_2), 2.05 (8H, m, CH_2), 1.18–1.05 (40H, m, CH_2), 0.79 (12H, t, *J* = 7, Me), 0.62–0.59 (8H, m, CH_2); δ_C (75 MHz; $CDCl_3$) 151.0 (C), 150.0 (C), 142.8 (C), 142.7 (C), 141.4 (C), 141.3 (C), 140.9 (C), 140.1 (C), 126.7 (CH), 126.6 (CH), 122.8 (CH), 119.2 (CH), 116.2 (2×CH), 113.8 (CH), 54.7 (C), 40.7 (CH_2), 36.6 (CH_2), 31.8 (CH_2), 30.1 (CH_2), 29.24 (CH_2), 29.23 (CH_2), 23.8 (CH_2), 22.5 (CH_2), 14.0 (Me).

2.2. Spectroscopic studies

Cyclohexane (ACS grade) and toluene (semiconductor grade) were purchased from Alfa Aesar. **LPP** (20 mg/mL in toluene, 90 μL)

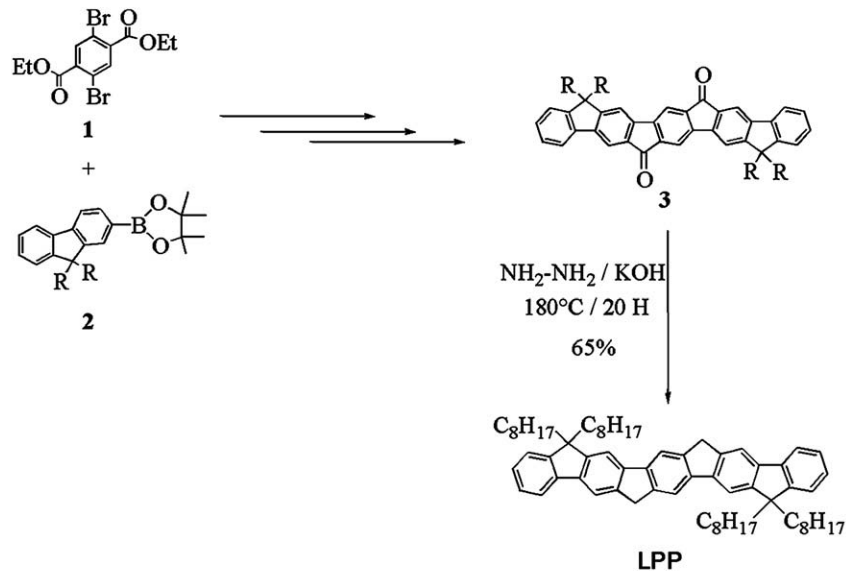

Scheme 1. Synthesis of **LPP**.

were deposited on quartz substrate using a 'home made' spin-coater and UV–visible and photoluminescence spectrum were immediately recorded. UV–visible spectra were recorded in thin film using a UV–visible spectrophotometer SHIMADZU UV-1605. UV–visible spectra were recorded in solution using either a UV–visible–NIR spectrophotometer CARY 5000-Varian (for quantum yield determination) or a UV–visible UVIKON XL Biotech spectrophotometer. The optical band gap was calculated from the absorption edge of the UV–vis absorption spectra in solution using the formula ΔE^{opt} (eV) $= hc/\lambda$, λ being the absorption edge (in meter). With $h = 6.626 \times 10^{-34}$ J s (1 eV $= 1.602 \times 10^{-19}$ J) and $c = 2.997 \times 10^{8}$ m s^{-1}. Photoluminescence spectra were recorded with a PTI spectrofluorimeter (PTI-814 PDS, MD 5020, LPS 220B) using a xenon lamp either in solution (cyclohexane) or in thin film. Quantum yields in solution (ϕ_{sol}) were calculated relative to quinine sulfate ($\phi_{sol} = 0.546$ in H_2SO_4 1 N) using standard procedures [23]. ϕ_{sol} was determined according to the following equation (1),

$$\phi_{sol} = \phi_{ref} \times 100 \times \frac{(T_s \times A_r)}{(T_r \times A_s)}\left(\frac{n_s}{n_r}\right)^2 \quad (1)$$

where subscripts s and r refer respectively to the sample and reference. The integrated area of the emission peak in arbitrary units is given as T, n is the refracting index of the solvent ($n_s = 1.42662$ for cyclohexane) and A is the absorbance. IR spectra were recorded on a BIORAD IRFTS175C.

2.3. Thermal analysis

Thermogravimetric analyses (TGA) were carried out with a Rigaku Thermoflex instrument under a nitrogen atmosphere between room temperature up to 1000 °C with a heating rate of 5 °C min^{-1}. Melting points were determined using an electrothermal melting point apparatus.

2.4. Electrochemical studies

All electrochemical experiments were performed under an argon atmosphere, using a Pt disk electrode (diameter 1 mm), the counter electrode was a vitreous carbon rod and the reference electrode was a silver wire in a 0.1 M $AgNO_3$ solution in CH_3CN. Ferrocene was added to the electrolyte solution at the end of a series of experiments. The ferrocene/ferrocenium (Fc/Fc^+) couple served as internal standard. For a further comparison of the electrochemical and optical properties, all potentials are referred to the SCE electrode that was calibrated at -0.405 V vs. Fc/Fc^+ system. The three electrode cell was connected to a PAR Model 173 potentiostat monitored with a PAR Model 175 signal generator and a PAR Model 179 signal coulometer. The cyclic voltammetry traces (CVs) were recorded on an XY SEFRAM-type TGM 164. CH_3CN with less than 5‰ of water (ref. SDS 00610S21) and CH_2Cl_2 with less than 100 ppm of water (ref. SDS 02910E21) were used without purification. Activated Al_2O_3 was added in the electrolytic solution to remove excess moisture. Following the work of Jenekhe [35], we estimated the electron affinity (EA) or lowest unoccupied molecular orbital (LUMO) and the ionisation potential (IP) or highest occupied molecular orbital (HOMO) from the redox data. The LUMO level was calculated from: LUMO (eV) $= -$[Eonset^{red} (*vs.* SCE) $+ 4.4$] and the HOMO level from: HOMO (eV) $= -$[Eonset^{ox} (*vs.* SCE) $+ 4.4$], based on an SCE energy level of 4.4 eV relative to the vacuum. The electrochemical gap was calculated from: $\Delta E^{el} = |$HOMO–LUMO$|$(in eV).

2.5. X-ray determination

The crystal was picked up with a cryoloop and then frozen at 100 K under a stream of dry N_2 on a APEX II Brucker AXS diffractometer for X-ray data collection (Mo Kα radiation, $\lambda = 0.71073$ Å). Structure was solved by direct methods (SIR97) [36] and refined (SHELXL-97) [37] by full-matrix least-squares methods as implemented in the WinGX software package [38]. An empirical absorption correction was applied. Hydrogen atoms were introduced at calculated positions (riding model) included in structure factor calculation but not refined. Crystallographic data have been deposited with the Cambridge Crystallographic Data Centre no. CCDC 713192. Copies of the data can be obtained free of charge on application to CCDC, 12 Union Road, Cambridge CB2 1EZ, UK [Fax: (+44) 1223-336-033; e-mail: deposit@ccdc.cam.ac.uk].

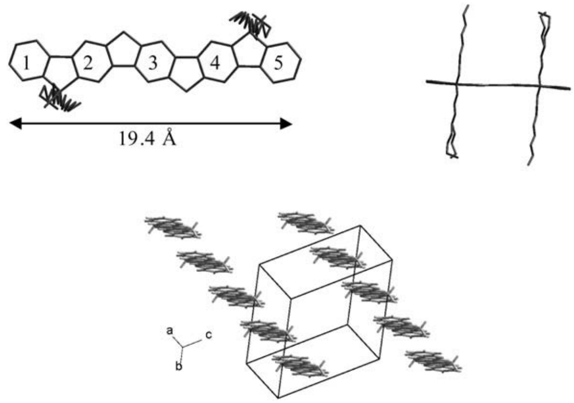

Fig 2. Top. Views of the molecular structure of **LPP** from single crystal X-Ray diffraction data (hydrogen atoms have been omitted for clarity); Bottom. Crystal packing diagram of **LPP**. The alkyl chains have been omitted for clarity.

2.5.1. Crystal data of LPP

$C_{68}H_{90}Cl_4$, $M = 1049.20$, triclinic, $a = 8.3174(11)$, $b = 13.5360(18)$, $c = 13.6781(16)$ Å, $\alpha = 105.180(6)$, $\beta = 90.561(5)$, $\gamma = 92.717(5)$ deg., $V = 1484.1(3)$ Å^3, $T = 100$ K, space group *P-1* (no. 2), $Z = 1$, 21 254 reflections measured, 6717 unique ($R_{int} = 0.0408$) which were used in all calculations. The final $wR(F^2)$ was 0.0896 (all data). More details of the final refinement are given in Supplementary information (SI).

3. Results and discussion

3.1. Synthesis

Starting from di-bromo terephthalate **1** [31] and 2-fluorene boronate **2** [32–34] and following a similar synthetic approach described by the Müllen group [3], the diketone **3** was prepared in a multistep synthesis as we already reported [24]. The diketone **3** was then involved in a Wolff-Kishner reduction, in diethylene glycol, in the presence of hydrazine in basic medium and led to **LPP** with 65% yield (Scheme 1).

3.2. Structural properties

Single crystals of **LPP** were obtained by liquid–liquid diffusion of MeOH into a solution of CH_2Cl_2. Single cristal X-ray diffraction experiments show that **LPP** crystallizes with one molecule of CH_2Cl_2, in the triclinic system, space group *P*-1, with the **LPP** unit on an inversion center and the CH_2Cl_2 molecule in general position. It should be noted that the four last atoms of one octyl chain were found to be disordered on two positions with 50% occupation factors. The pentaphenylene core, with a length of 19.4 Å, presents two distortions on both sides. The dihedral angles between the plane of the central phenyl ring 3 and those of the side rings 1 and 5 are of 6.5° (see phenyl rings labelling in Fig. 2-top). These distortions are larger than those reported by Wong [26] i.e. 2.5°, for an analogous tetra p-tolyl substituted ladder type oligopentaphenylene. However, these values are smaller than those we recently reported for the **DSF–LPP**, i.e. 8.4° [24].

As indicated in the crystal packing diagram of **LPP** presented in Fig. 2 (bottom), where the alkyls chains have been omitted for clarity, the pentaphenylene backbone are arranged in uniform stacks along the *a* axis. The intermolecular distance between the coplanar mean planes (through the central phenyl ring 3) of the pentaphenylene core was calculated to be around 3.6 Å. In the packing diagram, the distance between the plane of the phenyl ring 1 for one molecule and the centroid of the phenyl ring 3 of the neighbouring molecule was calculated to be 3.2 Å (see SI). This value appears to be the shortest distance between the centroid of one ring for one molecule and the plane of one ring for an other molecule. Moreover, the shortest ring–centroid/ring–centroid distance is evaluated to be around 4.3 Å (see SI). The **LPP** molecules are displaced with respect to each other and the slippage of the phenyl rings is also an important feature to find out about intermolecular interactions. We evaluated these different displacements as described by Janiak [39] and the angles lie between around 35° and 56° (see SI).[1] Moreover, several intermolecular short C–C distances were detected; the shortest being 3.39 Å (Fig. 3). In term of π stacking, atom–atom distances <3.6 Å are considered to moderately strong π–π interactions [39,40]. However it appears that only the edges of some rings slightly overlayed (Fig. 3, right) and then these interactions are likely C–H–π type and driven by the known $\pi-\sigma$ attraction [39]. Indeed, π-stacking interactions can be viewed as medium to weak if they exhibit rather long centroid–centroid distances (>4.0 Å) together with large slip angles (>30°) and vertical displacements ($d > 2.0$ Å). In contrast, strong π-stackings show rather short centroid–centroid contacts (<3.8 Å), small slip angles (<25°) and vertical displacements (<1.5 Å) which translate into a sizable overlap of the aromatic planes [39,41].

3.3. Optical properties

Optical properties of **DSF–LPP, DSF–IF** and **IF** have been already reported in our previous works and are presented here in the purpose of comparison [20,24].

The UV–Vis absorption spectrum of **LPP** (Fig. 4, left) presents a well defined vibronic structure with two main absorptions at 366 and 386 nm also observed in **DSF–LPP** (373 and 394 nm) with the latter being bathochromically shifted by *ca.* 7/8 nm (optical band gap ΔE^{opt}: 3.07 eV for **DSF–LPP** *vs.* 3.12 eV for **LPP**). A slightly higher bathochromic shift, 10 nm, has been also highlighted in the **IF** series, between **IF** and **DSF–IF**, Fig. 4-left. This shift arises from the interactions between the two orthogonally linked fluorene cores on the **LPP** or **IF** moieties [27,28,42,43]. Such red shift in UV–Vis spectra (among other properties) has been already stressed in spiro structures, by Johansson and coworkers [28]. Therefore and despite the orthogonality between the π-system 1 and the two π-systems 2, the chemistry involving one core is dependent to the other.

The main absorption band of the UV–Vis spectrum of **LPP** is also red shifted by 52 nm compared to the λ_{max} of **IF** (334 nm), Fig. 4-left. A strong decrease of the ΔE^{opt} is thus observed; 3.61 eV for **IF** *vs.* 3.12 eV for **LPP**. This clearly indicates that the degree of π conjugation is effectively extended in **LPP**. The emission spectrum of **LPP** ($\lambda_{exc} = 366$ nm, cyclohexane) presents two emission maxima recorded at 390 and 412 nm (Fig. 4, right), which are symmetrical to the absorption maxima. As expected, the Stokes shift is small and consistent with a highly rigid molecular structure, with only very small geometric changes during the transition from the ground to the excited state. When compared first to an analogous pentaphenylene derivative (**m1**) described by Advincula et al., (Scheme 2), bearing one phenyl ring and one hydrogen atom on each central bridge, a 5/7 nm red shift is observed ($\lambda_{em} = 395/419$ nm in $CHCl_3$) [25]. By replacing the previous hydrogen atom by an additional phenyl ring on each bridge i.e. a diaryl-substituted pentaphenylene (**m2**) (Scheme 2), an extra red shift is observed ($\lambda_{em} = 401/420$ nm in CH_2Cl_2) [6]. These results highlight (i) the importance of the bridges substitution and (ii) how the absorption and emission properties of such compounds may be tuned by an accurate substitution.

[1] Different angles and intermolecular ring–centroid/mean plane distances, ring–centroid/ring–centroid distances have been gathered in SI.

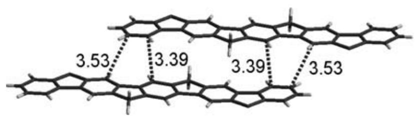

Fig. 3. View of the displacement of two molecules of **LPP** (portion of the crystal packing diagram). The alkyl chains have been omitted for clarity.

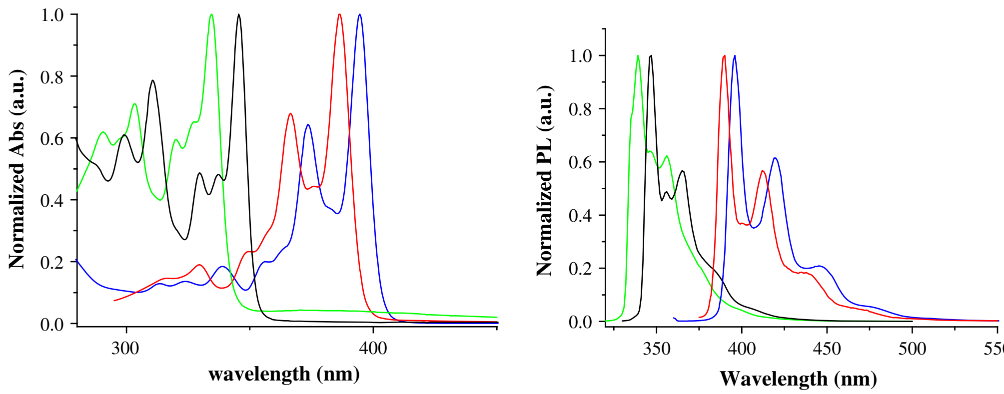

Fig. 4. Left. Normalized UV–Vis spectra of **IF** (green), **DSF–IF** (black), [20] **LPP** (red), **DSF–LPP** (blue) in solution in CH_2Cl_2 (10^{-5} M); Right. Normalized emission spectra of **IF** (green) in decalin, **DSF–IF** (black), [20] **LPP** (red), and **DSF–LPP** (blue) in cyclohexane. (For interpretation of the references to colour in figure legends, the reader is referred to the web version of this article.)

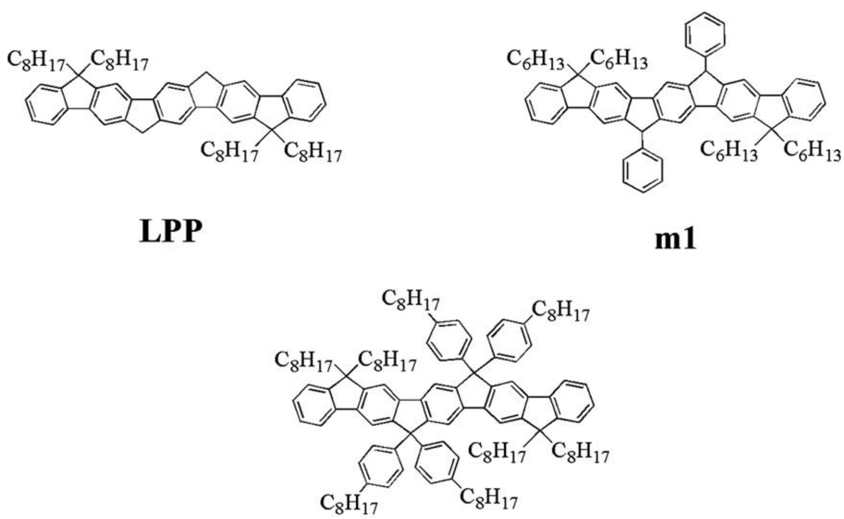

LPP

m1

m2

Scheme 2. Chemical structure of **LPP** and two other pentaphenylene derivatives, previously described by Advincula et al. (**m1**) [6] and by Müllen et al. (**m2**) [25].

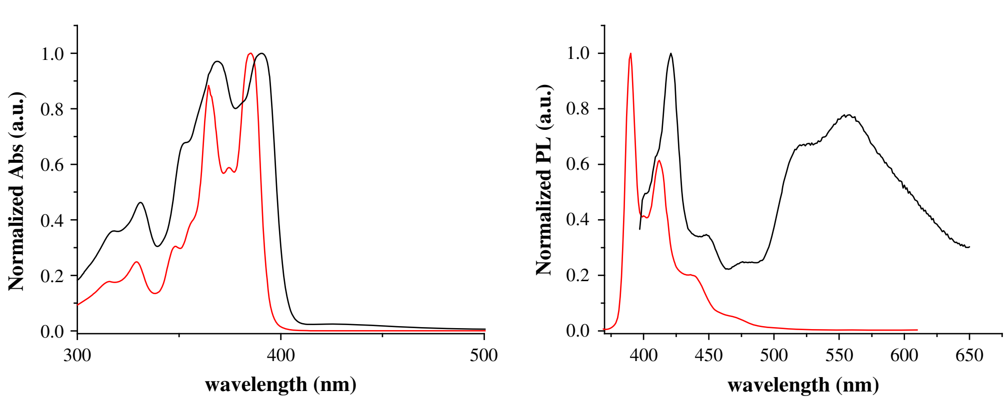

Fig. 5. Absorption (left) and photoluminescence (right, λ_{exc} = 330 nm) of **LPP** in solution in cyclohexane (red solid line) and in spin-coated thin film (black solid line). (For interpretation of the references to colour in figure legends, the reader is referred to the web version of this article.)

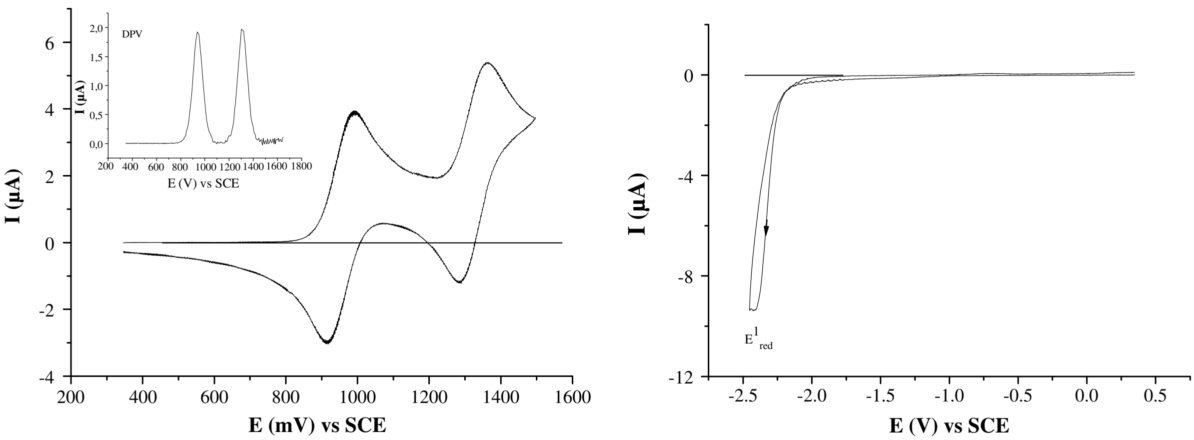

Fig. 6. CV of **LPP** (5×10^{-3} M) recorded in CH_2Cl_2 + Bu_4NPF_6 0.2 M. Platinum working electrode (diameter 1 mm), sweep-rate: 100 mV/s. Inset : DPV measurement of the oxidation.

Moreover, Müllen et al. recently assigned the two emission bands of the pentaphenylene **m2** to the 0–0 and 0–1 singlet transitions [6]. It is thus reasonable to assign the two emission maxima of **LPP** to the same transitions.

As observed in absorption, the same shift (8 nm) also exists between the two emission maxima of **IF** and **DSF–IF** and between the two emission maxima of **LPP** and **DSF–LPP**[2] highlighting the influence of the spiro-fluorene rings on the central backbone. We concluded that the trend is perfectly reproduced in the two series, either in absorption or in emission, as the effect of the two fluorene rings on the central core, whatever its length, appears to be very similar. Compared to **IF**, the emission maximum of **LPP** is red shifted by *ca.* 51 nm, signing again the extension of the π-system conjugation. The fluorescence quantum yield in solution, ϕ_{sol} was determined using standard procedures with quinine sulphate dihydrate as a reference [20,23], and appeared to be very high; *ca.* 81% for **LPP** *vs.* 65% for **IF** [20,23] indicating that the extension of conjugation has a direct influence on the quantum yield.

The UV–Vis thin film spectrum of **LPP** (Fig. 5, left) is broader but almost identical to its solution spectrum with a bathochromic shift of *ca.* 5–7 nm, which might be explained by the difference of dielectric constant of the environment [44,45]. In fluorescence, the same comparison reveals in the solid state, a loss of the fine vibronic structure, a 31 nm red shift and the appearance of a new broader emission band at *ca.* 515 and 556 nm (Fig. 5, right). A similar red shift (39 nm) was observed by Advincula et al. in the thin film fluorescence spectrum of **m1** (Scheme 2), attributed to the packing arrangement in the solid state [25]. However, no trace of a low-energy band was detected. On the other hand, pentaphenylene **m2** (Scheme 2) presents different behaviour, as the thin film fluorescence spectrum is almost identical to its solution spectrum, due to the presence of the two aryl substituents on the central bridges, which suppress aggregation and keto-defects.[6] Thus, the color stability in thin film gradually decreased from **m2** to **m1** and to **LPP** due to the presence of hydrogens at the bridgeheads. It is indeed obvious, due to the presence of the two easily oxidized methylene bridges, that **LPP** may easily lead to ketonic defects [2,46–49], probably mainly responsible of the presence of the low energy band in **LPP**.

3.4. Electrochemical properties

LPP oxidation (Fig. 6-left) presents first two reversible one-electron processes with maxima at 0.995 and 1.365 V *vs.* SCE. Confirmation of the isolectronic behaviour of these two oxidation waves was obtained by differential pulse voltammetry (DPV) (inset Fig. 6-left). The large potential difference between these signals reveals an efficient radical cation delocalization within the conjugated backbone as observed for other ladder pentaphenylene [26] and for **m2** [6]. The first and second oxidation were thus respectively assigned to the formation of a radical cation and a dication, both species being highly stable at the CV time scale. In the cathodic range, the reduction of **LPP** occurs at a highly negative potential close to the reduction wave of the supporting electrolyte (Fig. 6-right). This reduction wave is irreversible with an onset potential at −2.2 V *vs.* SCE. When comparing the intensity of the reduction wave to that of the oxidation, we concluded that this reduction process is bielectronic leading directly to the **LPP** dianion.

The LUMO and HOMO levels of **LPP** were estimated, from the reduction and oxidation onset potentials [35] to be respectively at −2.19 and −5.27 eV corresponding to an electrochemical band gap ΔE^{El} of 3.08 eV in accordance with the ΔE^{opt} (3.12 eV, *vide supra*). Comparing first **F**,[20] **IF** and **LPP**, the extension of the planar aromatic structure leads to a clear narrowing of the ΔE^{El} from 4.19 eV for **F**, to 3.63 eV for **IF**, and to 3.08 eV for **LPP**. This narrowing is due to the extension of the planar aromatic unit leading to a shift of both the HOMO and LUMO levels rendering the aromatic moiety more easily oxidized and reduced. Indeed, the HOMO level gradually increase from **F** (HOMO:−5.88 eV) to **IF** (HOMO: −5.62 eV) and to **LPP** (HOMO: −5.27 eV) and the inverse trend is observed for the LUMO levels; **F** (LUMO: −1.69 eV), **IF** (LUMO: −1.99 eV) and to **LPP** (LUMO: −2.19 eV). Moreover, the HOMO level of **LPP** is slightly higher than the one of **DSF–LPP**[24] (HOMO: −5.36 eV), as it was for **IF** compared to **DSF–IF**, signing the interactions of the fluorene units on the central aromatic backbone in the 3π−2 spiro structures.

LPP oxidation shows, at potential more anodic than 1.9 V, a third irreversible oxidation wave whose maximum is not observable before 2.5 V (Fig. 7-top). When this third oxidation process is reached, a polymerization process is observed leading to the appearance and the regular increase of reversible waves between 0.8 and 2.3 V along recurrent cycles, and by the coverage of the platinum electrode by an insoluble thin film.

Finally, after ten cycles (Fig. 7-top), the electrode surface is covered by an insoluble yellow-green deposit. After washing in CH_2Cl_2, the modified electrode has been studied in a monomer-free electrolytic solution that reveals the electrochemical behavior of poly(**LPP**) (Fig. 7-bottom). The E^{onset}_{ox} potential of poly(**LPP**) is recorded at 0.85 V, slightly lower than **LPP** (0.87 V), as observed along the electrodeposition process (*vide supra*). Electrochemical deposition processes have been already observed along anodic

[2] The two emission maxima of **DSF–LPP** have been observed at 397 and 420 nm [24].

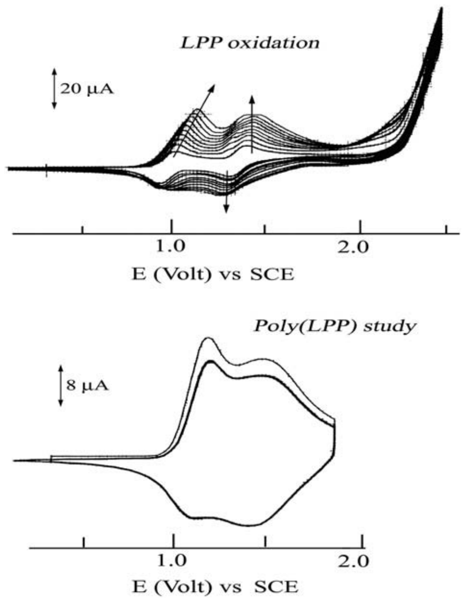

Fig. 7. CV in $CH_2Cl_2 + Bu_4NPF_6$ 0,2 M. Top. In the presence of **LPP**, ten sweeps between 0.2 and 2.5 V (showing the electrodeposition process). Working electrode: Platinum disk electrode (diameter 1 mm). Bottom. Three sweeps between 0.2 and 1.9 V in a solution free of any electroactive species (showing the poly(**LPP**) electroactivity). Sweep-rate: 100 mV/s. Working electrode: platinum disk modified by the film.

oxidation of **F** [29], **IF** [30], 2,7-oligofluorenes [50], and 9,9′-spirobifluorene [51–53].

Poly(**LPP**) is electrochemically stable and its oxidation is reversible in a potential range between 0.85 and 1.9 V. For comparison, poly(**IF**) [30] appears electroactive between 0.75 and 1.76 V, while poly(**F**) [50] presents a reversible p-doping process between 0.97 and 1.5 V and a second less reversible process between 1.5 and 1.8 V. The reversible p-doping process of poly(**LPP**) is described in Scheme 3 (right part).

The shift (20 mV) of the onset potential observed during the polymerization process of **LPP** is small when compared to what was observed during the polymerization of **F**[29] and 2,2′-di(9,9′-dialky**F**).[50] However, such small shift was also observed during **IF** and ter(9,9′-dialky**F**) polymerization. This might be explained by the fact that the conjugation lengths, in electrochemically generated poly(**LPP**), poly(**IF**) and poly(ter(9,9′-dialky**F**)), remain nearly the same than in their respective monomers. In the case of **LPP**, the charges are delocalized along five phenylene units both in **LPP** and in poly(**LPP**). Finally, when compared to other fluorene derivatives, **LPP** possesses an electropolymerization yield lower than their less extended analogues i.e. **F** [29] and **IF** [30].

Poly(**LPP**) does not show any n-doping process in the cathodic range up to −2.7 V. The cathodic exploration to such a negative potential does not damage the polymer, keeping its anodic electroactivity and thus reflecting its very high stability.

In the case of **LPP**, as already observed with di- and ter(9,9′-dialkyl**F**) [50]. the polymerization process occurs only at the third electron abstraction ($E^3{}_{ox}$). Indeed, the two first oxidation processes at $E^1{}_{ox}$ and $E^2{}_{ox}$ lead to stable charged species *(vide supra)* and may be described as presented in Scheme 3. Thus, neutral poly(**LPP**) consists in pentaphenylene units linearly linked through carbon–carbon bonds and belongs to the step-ladder-polyphenylene family described by Müllen [2]. To the best of our knowledge, this work is the first example of an electrochemical synthesis of a step-ladder-polyphenylene with four bridges [2].

Fig. 8-left shows the UV–Vis spectra of a **LPP** thin film and of poly(**LPP**) deposited along an oxidation at 2.5 V on an indium tin oxide (ITO) electrode. Poly(**LPP**) was either under its p-doped form (called p-doped poly(**LPP**)) or under its neutral form after reduction at 0 V (called neutral poly(**LPP**)). As presented before, **LPP** possess two strong absorption bands (369 and 391 nm) with an absorption edge at *ca.* 403 nm. Neutral poly(**LPP**) presents a larger spectrum with the two maxima being preserved (371 and 391 nm). Due to the broadness of the spectrum, the absorption edge is recorded at *ca.* 450 nm, bathochromically shifted by 50 nm compared to **LPP**. The UV–Vis spectrum of p-doped poly(**LPP**) is similar to the neutral poly(**LPP**), with the two same maxima. However, the spectrum also presents a broad absorption band with maxima at 510 and 550 nm, assigned to polaron and/or bipolaron species in the polymer backbone as already observed in poly(**F**) [54]. This additional band is observed in the same range than the absorption bands of the radical cations and dications of **LPP** electrogenerated in solution (Fig. 8-right). Indeed, the absorption bands of $\mathbf{LPP}^{\cdot+}$ and $\mathbf{LPP}^{2+}$ appeared between 400 and 600 nm (Fig 8-right). The regular increase of these new bands signs the high stability of the charged species on a large

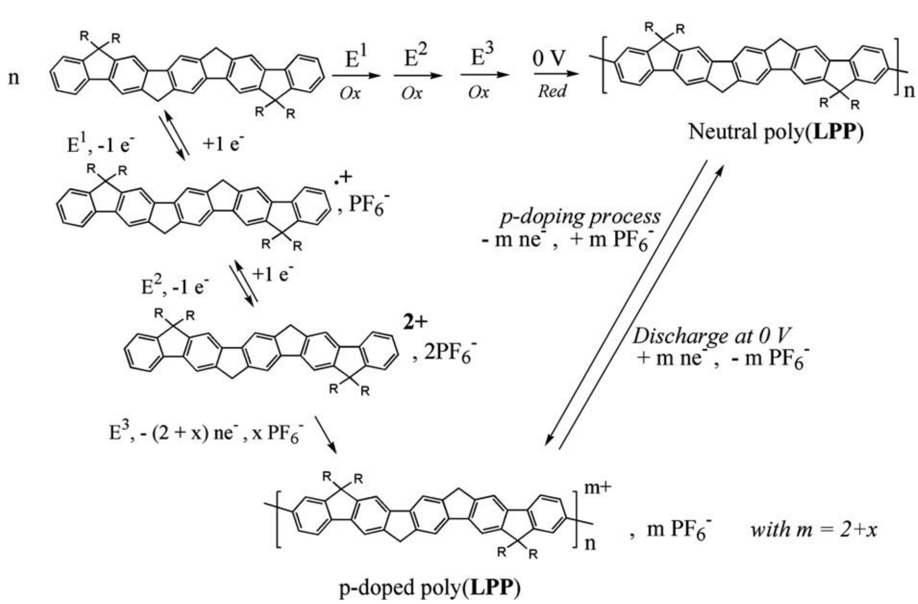

Scheme 3. Electrodeposition process and p-doping/undoping process of poly(**LPP**).

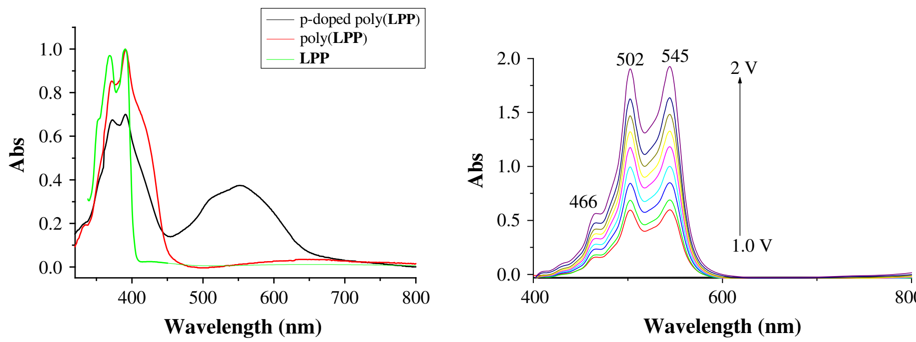

Fig. 8. Left. Absorption spectra of **LPP** in spin-coated thin film (green line), p-doped poly(**LPP**) (black line) and neutral poly(**LPP**) (red line). right. Spectroelectrochemical studies of the **LPP** anodic oxidation (between 1.0 and 2.0 V; step: 0.2 V) in $CH_2Cl_2 + Bu_4NPF_6$ 0.2 M. (For interpretation of the references to colour in figure legends, the reader is referred to the web version of this article.)

potential range (more than 1V). The similarity between the UV–Vis spectra of $\mathbf{LPP}^{\cdot+}/\mathbf{LPP}^{2+}$ and p-doped poly(**LPP**) leads us to conclude that the positive charges are delocalized on a similar aromatic structure on both monomer and polymer. This result is in accordance with the electrochemical conclusions.

To conclude, the thermal properties were evaluated by means of thermogravimetric analysis (TGA) under a nitrogen atmosphere at a rate of 5 °C min^{-1}. **LPP** presents a good thermal stability with a high decomposition temperature (*T*d, corresponding to 5% loss), i.e. 270 °C (see SI). This value is *ca.* 100 °C below the *T*d of its $3\pi-2$ spiro parent **DSF–LPP** i.e. 365 °C [24], highlighting the great improvement in term of stability obtains with the 'spiro' concept. Indeed, it is well known that spiro-linked derivatives are more stable than their non spiro counterpart [22].

4. Conclusion

In summary, we have synthesised a new ladder pentaphenylene (**LPP**), which is one of the simplest ladder type pentaphenylene ever prepared, bearing only two octyl chains on two bridgeheads. **LPP** is an attractive model compound as it can be seen as the central π-system of numerous pentaphenylenes, widely developed for electronic applications [3,6,25,26]. The structural, electrochemical and optical properties of **LPP** have been studied in detail and compared to previously reported pentaphenylenes. When comparing **DSF–LPP** and the central **LPP** unit, the present work confirms the existence, in the $3\pi-2$spiro compounds, of interactions between the different orthogonal π-systems; that is called spiroconjugation. As a similar observation has been previously performed when comparing **IF** and **DSF–IF**, we conclude that the trend is well reproduce in the two series. Finally, we have shown that the electrochemical oxidation of **LPP** leads to the formation of insoluble electroactive deposits on the working electrode surface. To the best of our knowledge, poly(**LPP**) is the first example of an electrochemically synthesized ladder-polyphenylene with four bridgeheads.

Acknowledgements

CP wishes to highly thank Prof. Dr. Janiak for helpful discussions about solid state interactions. N.C. thanks the Ministère de l'Education Nationale, de la Recherche et de la Technologie for a studentship. The authors would like to thank Dr Thierry Roisnel from the CDIFX (Centre de Diffractométrie X, UMR CNRS 6226-Rennes) for data collections, the C.R.M.P.O (Centre Régional de Mesure Physique de l'Ouest) for high resolution mass measurements and for CHN analysis. We also thank Dr Nathalie Audebrand for the TGA measurement and Damien Thirion and Stéphanie Fryars for invaluable technical assistance.

Appendix. Supplementary information

Supplementary information associated with this article can be found in the online version at doi:10.1016/j.dyepig.2009.06.001

References

[1] Thematic issue: organic electronics and optoelectronics. Chem Rev 2007;107:4.
[2] Grimsdale AC, Müllen K. Oligomers and polymers based on bridged phenylenes as electronic materials. Macromol Rapid Commun 2007;28:1676–702.
[3] Jacob J, Sax S, Piok T, List EJW, Grimsdale AC, Müllen K. Ladder-type pentaphenylenes and their polymers: efficient blue-light emitters and electron-accepting materials via a common intermediate. J Am Chem Soc 2004; 126:6987–95.
[4] Jacob J, Sax S, Gaal M, List EJW, Grimsdale AC, Müllen K. A fully aryl-substituted poly(ladder-type pentaphenylene): a remarkably stable blue-light-emitting polymer. Macromolecules 2005;38:9933–8.
[5] Schindler F, Jacob J, Grimsdale AC, Scherf U, Müllen K, Lupton JM, et al. Counting chromophores in conjugated polymers. Angew Chem Int Ed Engl 2005;44:1520–5.
[6] Zhou G, Baumgarten M, Müllen K. Arylamine-substituted oligo(ladder-type pentaphenylene)s: electronic communication between bridged redox centers. J Am Chem Soc 2007;129:12211–21.
[7] Mishra AK, Graf M, Grasse F, Jacob J, List EJW, Müllen K. Blue-emitting carbon- and nitrogen-bridged poly(ladder-type tetraphenylene)s. Chem Mater 2006;18:2879–85.
[8] Zhou G, Pschirer N, Schöneboom JC, Eickemeyer F, Baumgarten M, Müllen K. Ladder-type pentaphenylene dyes for dye-sensitized solar cells. Chem Mater 2008;20:1808–15.
[9] Zhu Y, Gibbons KM, Kulkarni AP, Jenekhe SA. Polyfluorenes containing dibenzo[*a*, *c*]phenazine segments: synthesis and efficient blue electroluminescence from intramolecular charge transfer states. Macromolecules 2007; 40:804–13.
[10] Tonzola CJ, Kulkarni AP, Gifford AP, Kaminsky W, Jenekhe SA. Blue-light-emitting oligoquinolines: synthesis, properties, and high-efficiency blue-light-emitting diodes. Adv Funct Mater 2007;17:863–74.
[11] Kim S-K, Park Y-I, Kang I-N, Park J-W. New deep-blue emitting materials based on fully substituted ethylene derivatives. J Mater Chem 2007;17:4670–8.
[12] Moorthy JN, Venkatakrishnan P, Huang D-F, Chow TJ. Blue light-emitting and hole-transporting amorphous molecular materials based on diarylaminobiphenyl-functionalized bimesitylenes. Chem Commun 2008:2146–8.
[13] Kim S-K, Yang B, Ma Y, Lee J-H, Park J-W. Exceedingly efficient deep-blue electroluminescence from new anthracenes obtained using rational molecular design. J Mater Chem 2008;18:3376–84.
[14] Tao S, Zhou Y, Lee C-S, Lee S-T, Huang D, Zhang X. Highly efficient nondoped blue organic light-emitting diodes based on anthracene–triphenylamine derivatives. J Phys Chem C 2008;112:14603–6.
[15] Tong Q-X, Lai S-L, Chan M-Y, Zhou Y-C, Kwong H-L, Lee C-S, et al. Highly efficient blue organic light-emitting device based on a nondoped electroluminescent material. Chem Mater 2008;20:6310–2.
[16] Qin T, Zhou G, Scheiber H, Bauer RE, Baumgarten M, Anson CE, et al. Polytriphenylene dendrimers: a unique design for blue-light-emitting materials. Angew Chem Int Ed Engl 2008;47:8292–6.
[17] Park Y-I, Son J-H, Kang J-S, Kim S-K, Lee J-H, Park J-W. Synthesis and electroluminescence properties of novel deep blue emitting 6,12-dihydro-diindeno[1,2-b;1′,2′-e]pyrazine derivatives. Chem Commun 2008:2143–5.

[18] Lai M-Y, Chen C-H, Huang W-S, Lin JT, Ke T-H, Chen L-Y, et al. Benzimidazole/amine-based compounds capable of ambipolar transport for application in single-layer blue-emitting OLEDs and as hosts for phosphorescent emitters. Angew Chem Int Ed Engl 2008;47:581–5.
[19] Wei Y, Chen C-T. Doubly ortho-linked *cis*-4,4'-bis(diarylamino)stilbene/fluorene hybrids as efficient nondoped, sky-blue fluorescent materials for optoelectronic applications. J Am Chem Soc 2007;129:7478–9.
[20] Poriel C, Liang J-J, Rault-Berthelot J, Barrière F, Cocherel N, Slawin AMZ, et al. Dispirofluorene-indenofluorene derivatives as new building blocks for blue organic electroluminescent devices and electroactive polymers. Chem Eur J 2007;13:10055–69.
[21] Poriel C, Rault-Berthelot J, Barrière F, Slawin AMZ. New dispiro compounds: synthesis and properties. Org Lett 2008;10:373–6.
[22] Saragi TPI, Spehr T, Siebert A, Fuhrmann-Lieker T, Salbeck J. Spiro compounds for organic optoelectronics. Chem Rev 2007;107:1011–65.
[23] Merlet S, Birau M, Wang ZY. Synthesis and characterization of highly fluorescent indenofluorenes. Org Lett 2002;4:2157–9.
[24] Cocherel N, Poriel C, Rault-Berthelot J, Barrière F, Audebrand N, Slawin AMZ, et al. New 3π-2spiro ladder-type phenylene materials: synthesis, physicochemical properties and applications in OLEDs. Chem Eur J 2008;14:11328–42.
[25] Xia C, Advincula RC. Ladder-type oligo(*p*-phenylene)s tethered to a poly(-alkylene) main chain: the orthogonal approach to functional light-emitting polymers. Macromolecules 2001;34:6922–8.
[26] Wong K-T, Chi L-C, Huang S-C, Liao Y-L, Liu Y-H, Wang Y. Coplanarity in the backbones of ladder-type oligo(*p*-phenylene) homologues and derivatives. Org Lett 2006;8:5029–32.
[27] King SM, Hintschich SI, Dai D, Rothe C, Monkman AP. Spiroconjugation-enhanced intramolecular charge-transfer state formation in a polyspirobifluorene homopolymer. J Phys Chem C 2007;111:18759–64.
[28] Johansson N, Dos Santos DA, Guo S, Cornil J, Fahlman M, Salbeck J, et al. Electronic structure and optical properties of electroluminescent spiro-type molecules. J Chem Phys 1997;107:2542–9.
[29] Rault-Berthelot J. Polyfluorenes, a family of versatile conjugated polymers. Anodic synthesis, physicochemical properties, electrochemical behaviour and application fields. Recent Res Dev Macromol Res 1998;3:425–37.
[30] Rault-Berthelot J, Poriel C, Justaud F, Barrière F. Anodic oxidation of indenofluorene. Electrodeposition of electroactive poly(indenofluorene). New J Chem 2008;32:1259–66.
[31] Lamba JJS, Tour JM. Imine-bridged planar poly(p-phenylene) derivatives for maximization of extended. π-conjugation. The common intermediate approach. J Am Chem Soc 1994;116:11723–36.
[32] Sonntag M, Kreger K, Hanft D, Strohriegl P, Setayesh S, de Leeuw D. Novel star-shaped triphenylamine-based molecular glasses and their use in OFETs. Chem Mater 2005;17:3031–9.
[33] Belletête M, Beaupré S, Bouchard J, Blondin P, Leclerc M, Durocher G. Theoretical and experimental investigations of the spectroscopic and photophysical properties of fluorene-phenylene and fluorene–thiophene derivatives: precursors of light-emitting polymers. J Phys Chem B 2000; 104:9118–25.
[34] Li T, Yamamoto T, Lan H-L, Kido J. Synthesis and electroluminescence properties of fluorene containing arylamine oligomer. Polym Adv Technol 2004;15:266–9.
[35] Kulkarni AP, Tonzola CJ, Babel A, Jenekhe SA. Electron transport materials for organic light-emitting diodes. Chem Mater 2004;16:4556–73.
[36] Altomare A, Cascarano G, Giacovazzo C, Guagliardi A, Burla MC, Polidori G, et al. *SIR*92-a program for automatic solution of crystal structures by direct methods. J Appl Cryst 1994;27:435–6.
[37] Sheldrick GM. SHELX97-programs for crystal structure analysis (Release 97-2); 1998.
[38] Farrugia L. *WinGX* suite for small-molecule single-crystal crystallography. J Appl Cryst 1999;32:837–8.
[39] Janiak C. A critical account on $\pi-\pi$ stacking in metal complexes with aromatic nitrogen-containing ligands. J Chem Soc, Dalton Trans 2000:3885–96.
[40] Nehls BS, Galbrecht F, Bilge A, Brauer DJ, Lehmann CW, Scherf U, et al. Synthesis and spectroscopy of an oligophenyl based cruciform with remarkable $\pi-\pi$ assisted folding. Org Biomol Chem 2003;3:3213–9.
[41] Yang X-J, Drepper F, Wu B, Sun W-H, Haehnel W, Janiak C. From model compounds to protein binding: syntheses, characterizations and fluorescence studies of [RuII(bipy)(terpy)L]2^+ complexes (bipy = 2,2′-bipyridine; terpy = 2,2′:6′,2″-terpyridine; L = imidazole, pyrazole and derivatives, cytochrome c). Dalton Trans 2005:256–67 [and references therein].
[42] Lukes V, Solc R, Milota F, Sperling J, Kauffmann HF. Theoretical investigation of the structure and the electron-vibrational dynamics of 9,9′-spirobifluorene. Chem Phys 2008;349:226–33.
[43] Boo BH, Choi YS, Kim T-S, Kang SK, Kang YH, Lee SY. Theoretical and jet spectroscopic investigations of energetics and structures for the low-lying singlet states of fluorene and 9,9′-spirobifluorene. J Mol Structure 1996; 377:129–36.
[44] Salbeck J, Yu N, Bauer J, Weissörtel F, Besten H. Low molecular organic glasses for blue electroluminescence. Synth Met 1997;91:209–15.
[45] Etori H, Jin XL, Yasuda T, Mataka S, Tsutsui T. Spirobifluorene derivatives for ultraviolet organic light-emitting diodes. Synth Met 2006;156:1090–6.
[46] Keivanidis PE, Jacob J, Oldridge L, Sonar P, Carbonnier B, Balutschev, et al. Photophysical characterization of light-emitting poly(indenofluorene)s. Chem Phys Chem 2005;6:1650–60.
[47] Romaner L, Heimel G, Wiesenhofer H, Scandiucci de Freitas P, Scherf U, Brêdas JL, et al. Ketonic defects in ladder-type poly(*p*-phenylene)s. Chem Mater 2004;16:4667–74.
[48] Gaal M, List EJW, Scherf U. Excimers or emissive on-chain defects? Macromolecules 2003;36:4236–7.
[49] Montilla F, Mallavia R. On the origin of green emission bands in fluorene-based conjugated polymers. Adv Mater 2007;17:71–8.
[50] Hapiot P, Lagrost C, Le Floch F, Raoult E, Rault-Berthelot J. Comparative study of the oxidation of fluorene, 9,9-disubstituted-fluorenes and of their related 2,7′-dimer and trimer. Chem Mater 2005;17:2003–12.
[51] Rault-Berthelot J, Granger MM, Mattiello L. Anodic oxidation of 9,9′-spirobifluorene in CH_2Cl_2 + 0.2 M Bu_4NBF_4. Electrochemical behaviour of the derived oxidation product. Synth Met 1998;97:211–5.
[52] Poriel C, Ferrand Y, Le Maux P, Rault-Berthelot J, Simonneaux G. Poly(9,9′-spirobifluorene-manganese porphyrin):a new catalytic material for oxidation of alkenes by iodobenzene diacetate and iodosylbenzene. Chem Commun 2003:1104–5.
[53] Poriel C, Ferrand Y, Le Maux P, Rault-Berthelot J, Simonneaux G. Organic cross-linked electropolymers as supported oxidation catalysts: poly(tetrakis(9,9′-spirobifluorenyl)porphyrin)manganese films. Inorg Chem 2004;43:5086–95.
[54] Rault-Berthelot J, Questaigne V, Simonet J, Peslerbe G. A new device for the in situ UV–visible spectroelectrochemical study of polymeric films set on solid surfaces: application to the study of the electrochemical behaviour of polyfluorenes. New J Chem 1989;13:45–52.